FERMILAB-PUB-19-382-AD-APC-ND-PPD

First demonstration of ionization cooling by the Muon Ionization Cooling Experiment

MICE collaboration

High-brightness muon beams of energy comparable to those produced by state-of-the-art electron, proton and ion accelerators have yet to be realised. Such beams have the potential to carry the search for new phenomena in lepton-antilepton collisions to extremely high energy and also to provide uniquely well-characterised neutrino beams. A muon beam may be created through the decay of pions produced in the interaction of a proton beam with a target. To produce a high-brightness beam from such a source requires that the phase space volume occupied by the muons be reduced (cooled). Ionization cooling is the novel technique by which it is proposed to cool the beam. The Muon Ionization Cooling Experiment collaboration has constructed a section of an ionization cooling cell and used it to provide the first demonstration of ionization cooling. We present these ground-breaking measurements.

Fundamental insights into the structure of matter and the nature of its elementary constituents have been obtained using beams of charged particles. The use of time-varying electromagnetic fields to produce sustained acceleration was pioneered in the 1930s [1–6]. Since then, high-energy and high-brightness particle accelerators have delivered electron, proton, and ion beams for applications that range from the search for new phenomena in the interactions of quarks and leptons, to the study of nuclear physics, materials science, and biology.

Muon beams are created using a proton beam striking a target to produce a secondary beam comprising many particle species including pions, kaons and muons. The pions and kaons decay to produce additional muons that are captured by electromagnetic beamline elements to produce a tertiary muon beam. Capture and acceleration must be realised on a time scale compatible with the $2.2\,\mu$s muon lifetime at rest. The energy of the muon beam is limited by the energy of the primary proton beam and the intensity is limited by the efficiency with which muons are accepted into the transport channel. High-brightness muon beams have not yet been produced at energies comparable to state-of-the-art electron and proton beams.

Accelerated high-brightness muon beams have been proposed as a source of neutrinos at a neutrino factory and to deliver multi-TeV lepton-antilepton collisions at a muon collider [7–13]. Muons have properties that make them ideal candidates for the delivery of high energy collisions. The muon is a fundamental particle with mass 207 times that of the electron, making collisions possible between beams of muons and antimuons at energies far in excess of those that can be achieved in an electron-positron collider such as the proposed International Linear Collider [14], the Compact Linear Collider [15–17] or the electron-positron option of the Future Circular Collider [18]. The energy available in collisions between the constituent gluons and quarks in proton-proton collisions is significantly less than the proton-beam energy because the colliding quarks and gluons each carry only a fraction of the proton's momentum. This makes muon colliders attractive to take the study of particle physics beyond the reach of facilities such as the Large Hadron Collider [19].

Most of the proposals for accelerated muon beams exploit the proton-driven muon beam production scheme outlined above. In these proposals the tertiary muon beam has its brightness increased through beam cooling before it is accelerated and stored. Four cooling techniques are in use at particle accelerators: synchrotron radiation cooling [20]; laser cooling [21–23]; stochastic cooling [24, 25]; and electron cooling [26]. In each case the time taken to cool the beam is long compared to the muon lifetime. Frictional cooling of muons, in which muons are electrostatically accelerated through an energy-absorbing medium at energies significantly below an MeV, has been demonstrated but only with low efficiency [27–30].

This document was prepared by [MICE Collaboration] using the resources of the Fermi National Accelerator Laboratory (Fermilab), a U.S. Department of Energy, Office of Science, HEP User Facility. Fermilab is managed by Fermi Research Alliance, LLC (FRA), acting under Contract No. DE-AC02-07CH11359

The novel technique demonstrated in this paper, ionization cooling [31, 32], is expected to occur when a suitably prepared beam passes through an appropriate material (the absorber) and loses momentum through ionization. Radio-frequency cavities restore momentum along the beam direction only. Passing the muon beam through a repeating lattice of material and accelerators causes the ionization cooling effect to build up in a time much shorter than the muon lifetime [33–35]. Acceleration of a muon beam in a radio-frequency accelerator has recently been demonstrated [36] and reduced beam heating, damped by the ionization cooling effect, has been observed [37]. However, ionization cooling has never previously been demonstrated. Such a confirmation is important for the development of future muon accelerators. The international Muon Ionization Cooling Experiment (MICE) [38] was designed to demonstrate transverse ionization cooling, the first observation of which is presented here. The brightness of a particle beam can be characterised by the number of particles in the beam and the volume occupied by the beam in position-momentum phase space. The phase space considered in this paper is the position and momentum transverse to the direction of travel of the beam: $\mathbf{u} = (x, p_x, y, p_y)$, where x and y are coordinates perpendicular to the beam line, and p_x and p_y are the corresponding components of momentum. The z-axis is the nominal beam axis.

The phase space volume occupied by the beam and the phase space density of the beam are conserved quantities in a conventional accelerator without cooling. The normalised root-mean-square (RMS) emittance is often used as an indicator of the phase space volume occupied by the beam and is given by [39]

$$\varepsilon_\perp = \frac{\sqrt[4]{|\mathbf{V}|}}{m_\mu}, \tag{1}$$

where m_μ is the muon mass and $|\mathbf{V}|$ is the determinant of the covariance matrix of the beam in transverse phase space. The covariance matrix has elements $v_{ij} = \langle u_i u_j \rangle - \langle u_i \rangle \langle u_j \rangle$. The distribution of individual particle amplitudes also describes the volume of the beam in phase space. The amplitude is defined by [40]

$$A_\perp = \varepsilon_\perp R^2(\mathbf{u}, \langle \mathbf{u} \rangle), \tag{2}$$

where $R^2(\mathbf{u}, \mathbf{v})$ is the square of the distance between two points, $\mathbf{u}$ and $\mathbf{v}$, in the phase space, normalised to the covariance matrix:

$$R^2(\mathbf{u}, \mathbf{v}) = (\mathbf{u} - \mathbf{v})^T \, \mathbf{V^{-1}} \, (\mathbf{u} - \mathbf{v}). \tag{3}$$

The normalised RMS emittance is proportional to the mean of the particle amplitude distribution. In the approximation that particles travel near to the beam axis, and in the absence of cooling, the particle amplitudes and the normalised RMS emittance are conserved quantities. If the beam is well described by a multivariate Gaussian distribution then R^2 is distributed according to a χ^2 distribution with four degrees of freedom so the amplitudes are distributed according to

$$f(A_\perp) = \frac{A_\perp}{4\varepsilon_\perp^2} \exp\left(\frac{-A_\perp}{2\varepsilon_\perp}\right). \tag{4}$$

The rate of change of the normalised transverse emittance as the beam passes through an absorber is given approximately by [32, 39, 41]

$$\frac{d\varepsilon_\perp}{dz} \backsimeq -\frac{\varepsilon_\perp}{\beta^2 E_\mu} \left|\frac{dE_\mu}{dz}\right| + \frac{\beta_\perp (13.6\,\mathrm{MeV}/c)^2}{2\beta^3 E_\mu m_\mu X_0}, \tag{5}$$

where βc is the muon velocity, E_μ the energy, $\left|\frac{dE_\mu}{dz}\right|$ the mean energy loss per unit path length, X_0 the radiation length of the absorber and $\beta_\perp$ the transverse betatron function at the absorber [39]. The first term of this equation describes 'cooling' by ionization energy loss and the second describes 'heating' by multiple Coulomb scattering. Equation 5 implies that there is an equilibrium emittance for which the emittance change is zero.

If the beam is well described by a multivariate gaussian distribution both before and after cooling then the downstream and upstream amplitude distributions $f^d(A_\perp)$ and $f^u(A_\perp)$ are related to the downstream and upstream emittances $\varepsilon_\perp^d$ and $\varepsilon_\perp^u$ by

$$\frac{f^d(A_\perp)}{f^u(A_\perp)} = \left(\frac{\varepsilon_\perp^u}{\varepsilon_\perp^d}\right)^2 \exp\left[-\frac{A_\perp}{2}\left(\frac{1}{\varepsilon_\perp^d} - \frac{1}{\varepsilon_\perp^u}\right)\right]. \tag{6}$$

Many particles in the experiment described in this paper do not travel near to the beam axis. These particles experience effects from optical aberrations, as well as geometrical effects such as scraping, in which

high amplitude particles outside the experiment's aperture are removed from the beam. Scraping reduces the emittance of the ensemble, and selectively removes those particles that scatter more than the rest of the ensemble. Optical aberrations and scraping introduce a bias in the change in RMS emittance that occurs due to ionization cooling. In this paper the distribution of amplitudes is studied. In order to expose the behaviour in the beam core, independently of aberrations affecting the beam tail, $\mathbf{V}$ and $\varepsilon_\perp$ are recalculated for each amplitude bin, including particles that are in lower amplitude bins and excluding particles that are in higher amplitude bins. This results in a distribution that, in the core of the beam, is independent of scraping effects and aberrations.

Change in phase space density provides a direct measurement of the cooling effect. The k-Nearest Neighbour (kNN) algorithm provides a robust non-parametric estimator of the phase space density of the muon ensemble [42, 43]. The separation of pairs of muons is characterised by the normalised squared distance, $R^2_{ij}(\mathbf{u}_i, \mathbf{u}_j)$, between muons with position $\mathbf{u_i}$ and $\mathbf{u_j}$. The density, ρ_i, associated with the i^{th} particle is estimated by

$$\rho_i(\mathbf{u_i}) = \frac{k}{n|\mathbf{V}|^{\frac{1}{2}}}\frac{1}{v_{ik}} = \frac{2k}{n\pi^2|\mathbf{V}|^{\frac{1}{2}}}\frac{1}{R^4_{ik}}\,, \qquad (7)$$

where v_{ik} is the volume of the hypersphere, centred on $\mathbf{u}_i$, that intersects the particle having the k^{th} smallest R_{ij} and n is the number of particles in the ensemble. An optimal value for k has been used, $k = n^{4/(4+d)} = \sqrt{n}$, with phase space dimension $d = 4$ [43].

The MICE collaboration has built a tightly focusing solenoid lattice, absorbers and instrumentation to demonstrate ionization cooling of muons. A schematic of the apparatus is shown in figure 1.

A transfer line [44–46] brought a beam, composed mostly of muons, from a target [47] in the ISIS synchrotron [48] to the cooling apparatus. The muons had a nominal momentum of 140 MeV/c. A variable thickness brass and tungsten diffuser allowed the incident beam emittance to be varied between 4 and 10 mm.

The tight focussing (low beta function) and large acceptance required by the cooling section was achieved using twelve superconducting solenoids. The solenoids were contained in three warm-bore modules cooled by closed cycle cryocoolers. The upstream and downstream modules (the 'spectrometer solenoids') were identical, each containing three coils to provide a uniform field region of up to 4T within the 400 mm diameter warm bore for momentum measurement, and two 'matching' coils to match the beam to the central pair of closely spaced 'focus' coils which focussed the beam onto the absorber. The focus coils were a pair of split-field coils designed for peak on-axis fields of up to 3.5 T contained within one module with a 500 mm diameter warm bore which contained the absorbers. For the data reported here the focus coils were operated in 'flip' mode with a field reversal at the centre. Because the magnetic lattice was tightly coupled the cold mass suspension systems of the modules were designed to withstand the longitudinal cold-to-warm forces of several hundred kN which could arise during an unbalanced quench of the system. At maximum field the inter-coil force on the focus coil cold mass was of the order of 2 MN. The total energy stored in the magnetic system was of the order of 5 MJ and the system was protected by both active and passive quench protection systems. The normal charging and discharging time of the solenoids was several hours. The entire magnetic channel was partially enclosed by a 150 mm thick soft-iron return yoke for external magnetic shielding. The magnetic fields in the tracking volumes were monitored during operation with calibrated Hall probes.

One of the matching coils in the downstream spectrometer solenoid was not operable due to a failure of a superconducting lead. While this necessitated a compromise in the lattice optics and acceptance, the flexibility of the magnetic lattice was exploited to ensure a clear cooling measurement.

The amplitude acceptance of approximately 30 mm, above which particles scrape, was large compared to a typical accelerator. Even so significant scraping was expected and observed for the highest emittance beams. Ionization cooling cells with even larger acceptances, producing less scraping, have been designed [33–35]. The magnetic lattice of MICE was tuned so that the beam had a focus near to the absorber resulting in a small beam width, shown in figure 1, and large angular divergence. The tight focussing, corresponding to a region of small $\beta_\perp$, yielded an optimal

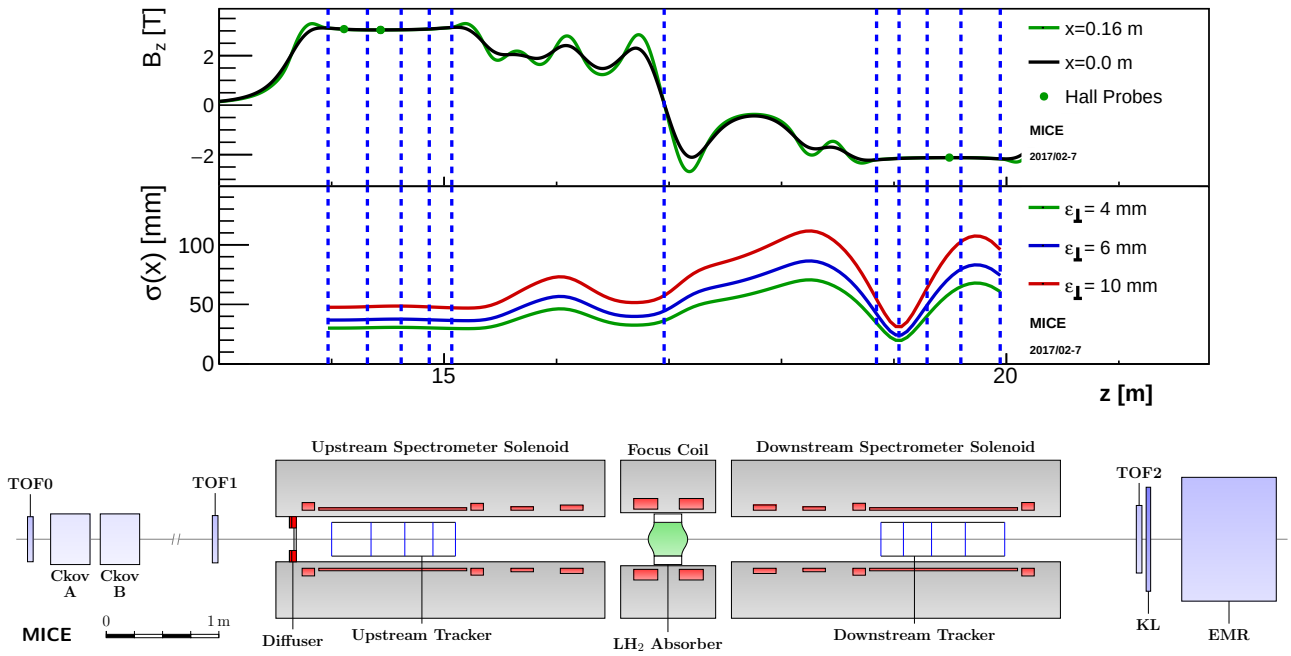

Figure 1: The MICE apparatus along with the calculated magnetic field, B_z [T], and nominal horizontal width of the beam, $\sigma(x)$ [mm]. The modelled field is shown on the beam axis and 160 mm from the axis in the horizontal plane. The readings of Hall probes, situated 160 mm from the beam axis, are also shown. Dashed lines indicate the position of the tracker stations and absorber. The nominal RMS beam width is calculated assuming a nominal input beam using linear beam transport equations. Acronyms used in the schematic are described in the text.

cooling performance, as implied by equation 5.

Materials with low atomic number such as lithium and hydrogen have a long radiation length relative to the rate of energy loss and consequently low equilibrium emittance, making them ideal absorber materials. Therefore the cooling due to both liquid hydrogen and lithium hydride absorbers was studied.

The liquid hydrogen was contained within a 22 l vessel [49] in the warm bore of the focus coil. Hydrogen was liquefied by a cryocooler and piped through the focus coil module into the absorber body. When filled, the absorber presented 349.6 ± 0.2 mm of liquid hydrogen along the beam axis with a density of 0.07053 ± 0.00008 g/cm^3. The liquid hydrogen was contained by a pair of aluminium windows covered by multi-layer insulation. A second pair of windows provided secondary containment to protect against the possibility of failure of the primary containment windows. The total thickness of all four windows on the beam axis was 0.79 ± 0.01 mm.

The lithium hydride absorber was a 65.37 ± 0.02 mm thick disk with a density of 0.6957 ± 0.0006 g/cm^3. The isotopic composition of the lithium used to produce the absorber was 95 % ^{6}Li and 5 % ^{7}Li. The cylinder had a thin coating of parylene to prevent ingress of water or oxygen. Configurations with no absorber installed at all and with the empty liquid hydrogen containment vessel were also studied.

Detectors placed upstream and downstream of the apparatus measured the momentum, position, and species of each particle entering and leaving the cooling channel so that the full four-dimensional phase space, including the angular momentum introduced by the solenoids, could be reconstructed. Particles were recorded by the apparatus one at a time, which enabled high-precision instrumentation to be used and particles other than muons to be excluded from the analysis. Each ensemble of muons was accumulated over a number of hours of operation of the experiment. This is acceptable as collective effects are not

expected at a neutrino factory and in a muon collider collective effects become significant only at very low longitudinal emittance [50]. Data-taking for each absorber was separated by a period of weeks due to operational practicalities. The phase space distribution of the resulting ensemble was reconstructed using the upstream and downstream detectors. Emittance reconstruction in the upstream detector system is described in [51].

Upstream of the cooling apparatus, two time-of-flight detectors (TOFs) [52, 53] measured particle velocity. A complementary velocity measurement was made upstream by threshold Cherenkov counters Ckov A and Ckov B [54]. Scintillating fibre trackers, positioned in the uniform-field region of each of the two spectrometer solenoids, measured particle position and momentum upstream and downstream of the absorber [45, 55, 56]. Downstream, an additional TOF detector, a mixed lead and scintillator pre-shower detector (KL), and a totally active scintillator calorimeter, the Electron Muon Ranger (EMR) [57, 58] identified electrons produced in muon decay and allowed cross-validation of the measurements made by the upstream detectors and the trackers.

Each tracker consisted of five planar scintillating fibre stations. Each station comprised three views, each view composed of scintillating fibres laid at an angle of 120° with respect to the other views. Each view was made of two layers of 350 μm diameter scintillating fibres. Groups of seven scintillating fibres were read out together by cryogenic Visible Light Photon Counters [59, 60]. The position of a particle crossing the tracker was inferred from the coincidence of signals from the fibres and momentum was inferred by fitting a helical trajectory to the positions with appropriate consideration for energy loss and scattering in the fibres.

Each TOF was constructed from two orthogonal planes of scintillator slabs. Photomultiplier tubes at each end of every TOF slab were used to determine the time at which a muon passed through the apparatus with a 60 ps resolution [52]. The momentum resolution of particles for which the radius of the helix in the tracker was small was improved by combining the TOF measurement of velocity with the measurement of momentum in the tracker.

A detailed Monte Carlo simulation of the experiment was performed to study the resolution and efficiency of the instrumentation and to determine the expected performance of the cooling apparatus [61–63]. The simulation was found to give a good description of the data [51].

The data presented here were taken using beams with a nominal momentum of 140 MeV/c and with a nominal normalised RMS emittance in the upstream tracking volume of 4 mm, 6 mm and 10 mm. These settings are denoted '4-140', '6-140' and '10-140' respectively. Beams with a higher emittance have correspondingly higher amplitude and occupy a larger region in phase space. For each beam setting, two samples were considered for the analysis. The 'upstream sample' contained particles identified as muons using the upstream TOF detectors and tracker, for which the muon trajectory reconstructed in the upstream tracker was fully contained in the fiducial volume and for which the reconstructed momentum fell within the range 135 MeV/c to 145 MeV/c, which was significantly larger than the 2 MeV/c momentum resolution of the tracker. The 'downstream sample' was that subset of the upstream sample for which the reconstructed muons were fully contained in the fiducial volume of the downstream tracker. The samples each had between 30,000 and 170,000 events. The distributions in phase space of the particles in the two samples are shown in figure 2. The strong correlations between y and p_x and between x and p_y are due to the angular momentum introduced by the solenoidal field. The shorter tail along the semi-minor axis than the semi-major axis in these projections arises from scraping in the diffuser.

The distribution of amplitudes in the upstream and downstream samples for each of the 4-140, 6-140, and 10-140 data sets is shown in figure 3. The nominal acceptance of the magnetic channel is also indicated. A correction has been made to account for the migration of events between amplitude bins that arises due to the detector resolution and to account for inefficiency in the downstream detector system. The correction is described in the Methods section. Distributions are shown for the case where there was no absorber ('No absorber'), where the liquid hydrogen vessel was empty ('Empty LH_2'), where the liquid hydrogen ves-

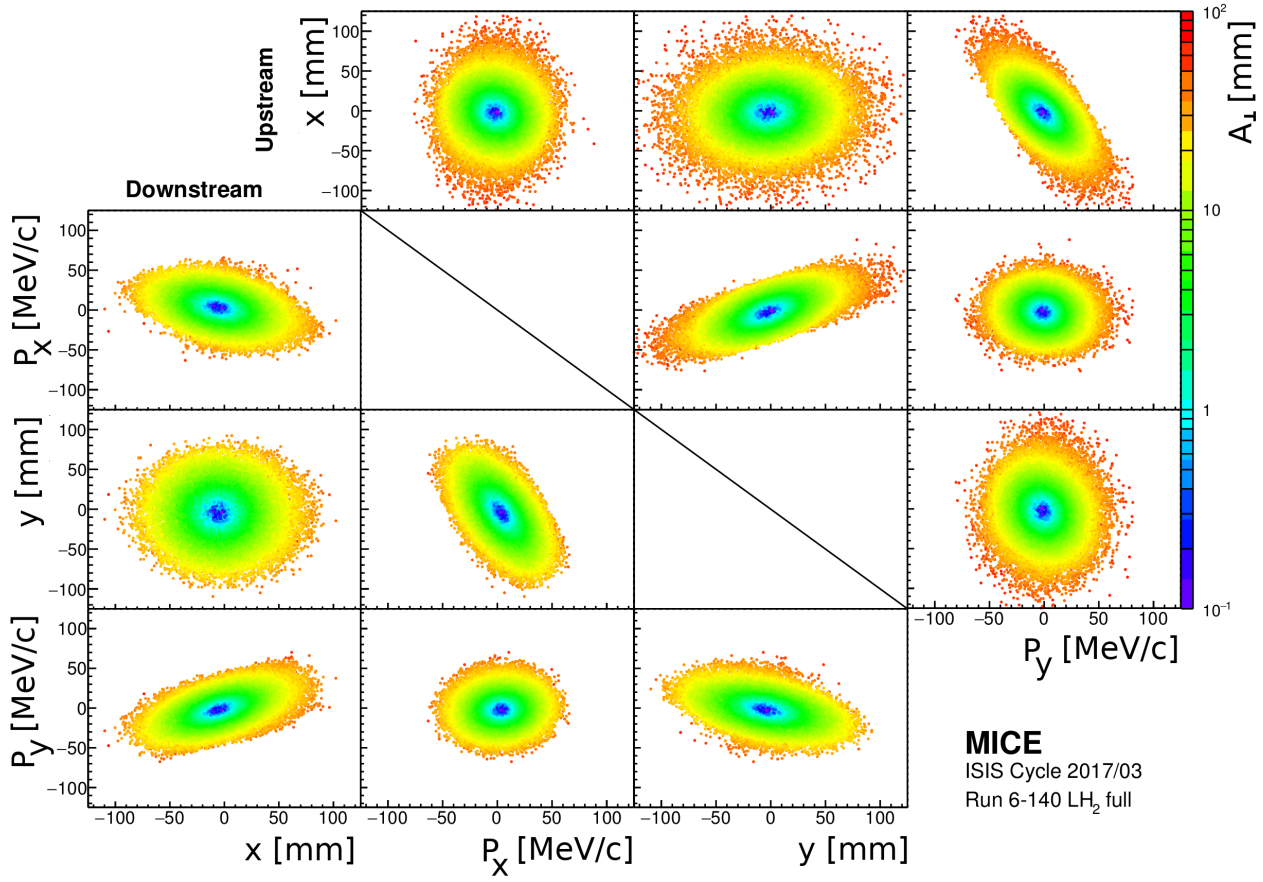

Figure 2: Distribution of the beam in phase space for the 6-140 Full LH_2 setting: (above the diagonal) measured in the upstream tracker and (below the diagonal) measured in the downstream tracker. Measured particles' positions are shown, coloured according to the amplitude of the particle.

sel was filled ('Full LH_2'), and where the lithium hydride absorber was present ('LiH'). The distributions were normalised to allow a comparison of the shape of the distribution between different absorbers. Each pair of upstream and downstream amplitude distributions is scaled by $1/N^u_{max}$, where N^u_{max} is the number of events in the most populated bin in the upstream sample.

The behaviour of the beam at low amplitude is the key result of this paper. For the 'No absorber' and the 'Empty LH_2' configurations, the number of events with low amplitude in the downstream sample is similar to that observed in the upstream sample. For the 6-140 and 10-140 configurations for both the 'Full LH_2' and the 'LiH' samples, the number of events with low amplitude is significantly larger in the downstream sample than in the upstream sample. This indicates an increase in the number of particles in the beam core when an absorber is installed, which is expected if ionization cooling occurs. This effect can only occur because energy loss due to ionization is a non-conservative process.

A reduction in the number of muons at high amplitude is also observed, especially for the 10-140 setting. While some of this effect arises due to migration of muons into the beam core, a significant number of high amplitude particles migrated away from the beam acceptance due to optical mismatch and were scraped on apertures.

A χ^2 test was performed to determine the confidence with which the null hypothesis that, for the same input beam setting, the amplitude distribution in the downstream samples of the 'Full LH_2' and 'Empty LH_2' configurations are compatible, and the amplitude distribution in the downstream samples of the 'LiH' and 'No absorber' configurations are compatible. The

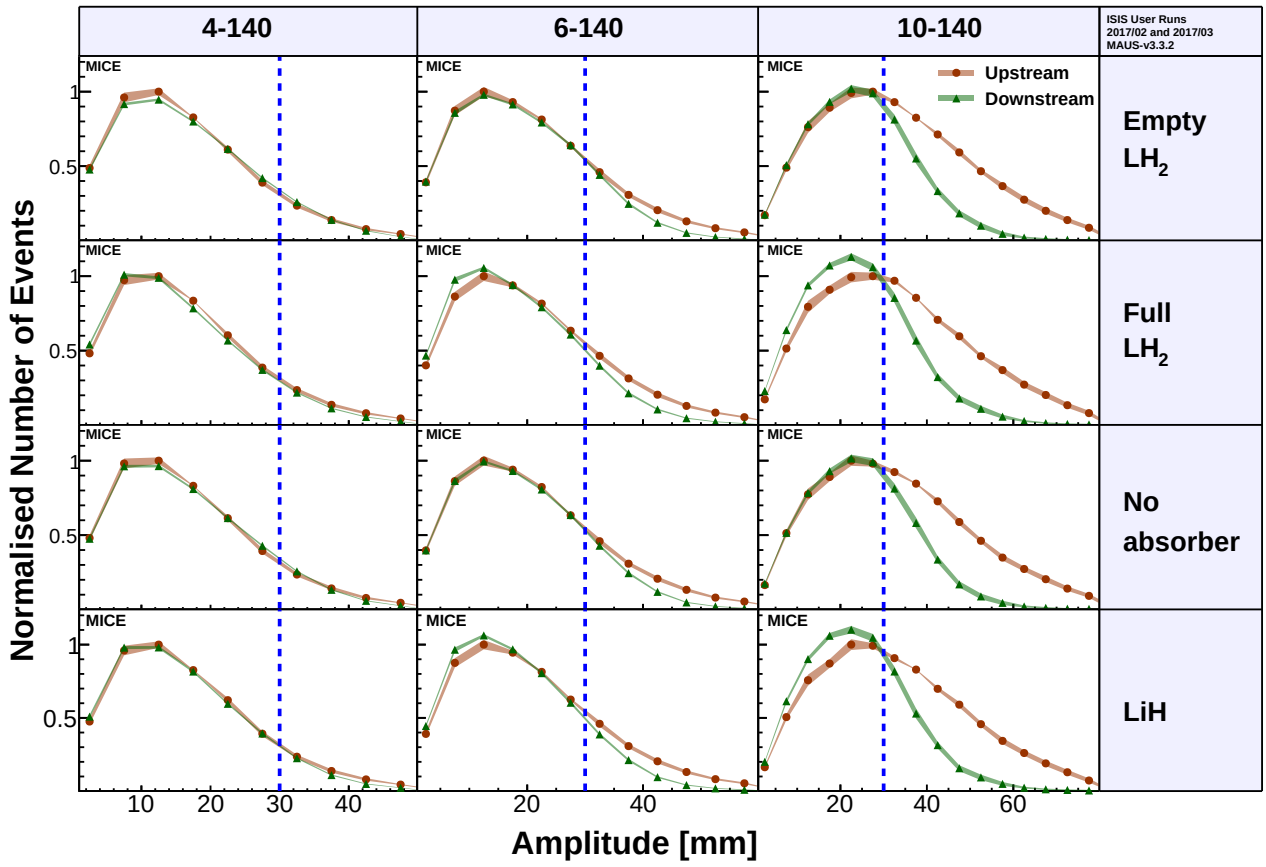

Figure 3: The distributions of measured muon amplitudes. The upstream distributions are shown by orange circles while the downstream distributions are shown by green triangles. Both upstream and downstream distributions are normalised to the bin in the upstream distribution with the most entries (see text). Coloured bands show the uncertainty, which is dominated by systematic uncertainties. Vertical lines indicate the approximate channel acceptance above which scraping occurs.

test was performed on the uncorrected distributions assuming statistical uncertainties only. Systematic effects are the same for the pairs of distributions tested and cancel. The probability of observing the effect seen in the data, assuming this null hypothesis is correct, is significantly less than 10^{-5} for all beam settings and all pairs of 'Full LH_2' and 'Empty LH_2' and all pairs of 'LiH' and 'No absorber', therefore the null hypothesis was rejected.

The fractional increase in the number of particles with low amplitude is most pronounced for the 10-140 beams. High amplitude beams have high $\varepsilon_\perp$ and a larger transverse momentum relative to the stochastic increase in transverse momentum due to scattering, so undergo more cooling, as predicted by equation 5. For the magnet settings and beams studied here the equilibrium emittance of the experiment is close to 4 mm. As a result only modest cooling is observed for the 4-140 setting in both the 'Full LH_2' and the 'LiH' configuration.

The ratio of the downstream to the upstream amplitude distribution is shown in figure 4. In the 'No absorber' and 'Empty absorber' configurations, the ratio is consistent with 1 for amplitudes less than 30 mm, confirming the conservation of amplitude in this region irrespective of the incident beam. Above 30 mm the ratio drops below unity, indicating that there are fewer muons downstream than upstream due to the

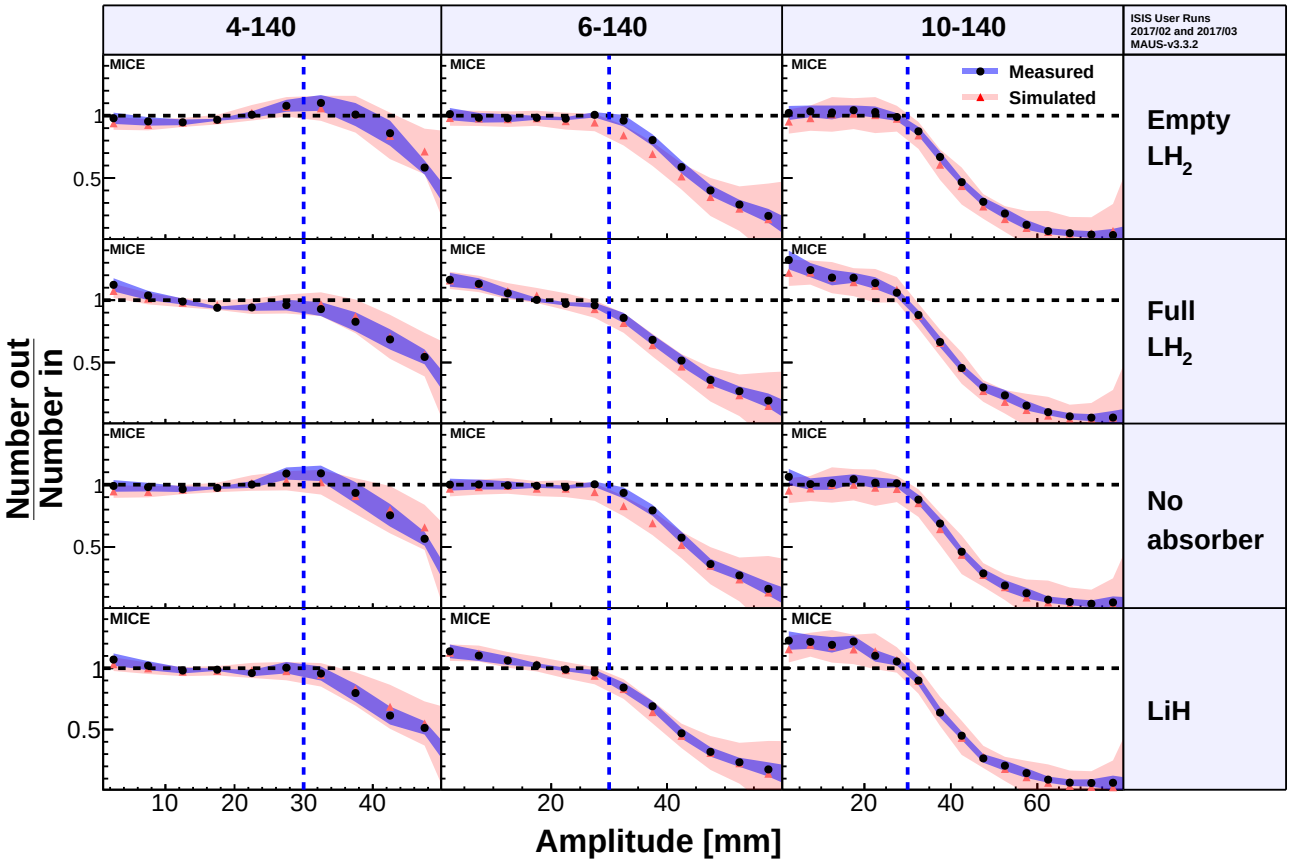

Figure 4: Downstream to upstream ratio of number of events. A ratio greater than unity in the beam core is evidence for ionization cooling and is evident for 6-140 and 10-140 beams with both the full LH_2 absorber and the LiH absorber. The effect predicted from simulation is shown in red, while that measured is shown in black. Uncertainty is shown by a blue fill for data and a pink fill for simulation and is dominated by systematic uncertainty. Vertical lines indicate the channel acceptance above which scraping occurs.

beam scraping on apertures. The presence of the absorber windows does not strongly affect the amplitude distribution. The liquid hydrogen absorber windows were designed to be as thin as possible so that when installed, scattering in the windows would not cause significant heating. For the 6-140 and 10-140 data sets, the addition of liquid hydrogen or lithium hydride absorber material causes the ratio to rise above unity for low amplitude particles, corresponding to the beam core. This indicates an increase in the number of particles in the beam core and demonstrates ionization cooling.

The density in phase space is an invariant of a symplectic system, therefore an increase in phase space density is also an unequivocal demonstration of cooling. Figure 5 shows the normalised density of the beam $\rho_i(\mathbf{u_i})/\rho_0$ as a function of α, the fraction of the upstream sample that has a density greater than or equal to ρ_i. To enable comparison between different beam configurations, the densities for each configuration have been normalised to the peak density in the upstream tracker, ρ_0. To enable comparison between upstream and downstream distributions, the fraction of the sample is always relative to the total number of events in the upstream sample. The transmission is the fraction of the beam where the density

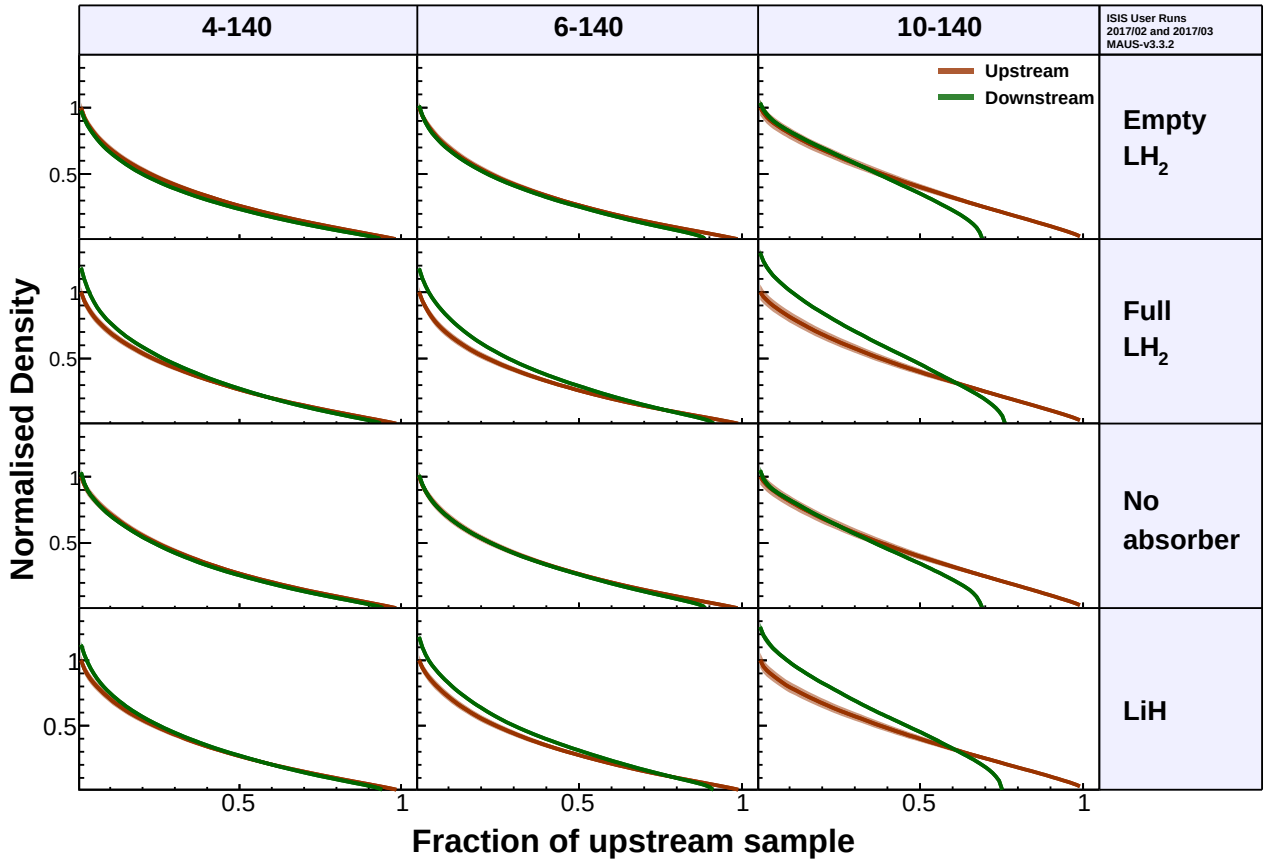

Figure 5: The upstream and downstream normalised beam density quantiles, indicated by orange and green lines respectively, as a function of the fraction of the upstream sample. For each configuration, the density is normalised to the highest density region in the upstream sample. Uncertainty is indicated by the thickness of the coloured bands and is dominated by systematic uncertainty.

in the downstream tracker reaches zero. For the 'No absorber' and 'Empty LH_2' cases the density downstream in the highest density regions is indistinguishable from the density upstream. A small amount of scraping is observed for the 4-140 and 6-140 beams. More significant scraping is observed for the 10-140 beam. In all cases, for 'Full LH_2' and 'LiH', the phase space density increases. The increase is more significant for higher emittance beams. These observations demonstrate the ionization cooling of the beam when an absorber is installed. In the presence of an absorber, beams with larger nominal emittance show a greater increase in density than those with a lower nominal emittance, which is consistent with equation 5.

Ionization cooling has been unequivocally demonstrated for the first time. The MICE collaboration has built and operated a section of solenoidal cooling channel and demonstrated the ionization cooling of muons using both liquid hydrogen and lithium hydride absorbers. The effect has been observed both from observation of an increase in the number of particles having a small amplitude (figures 3 and 4) and an increase in the phase space density of the beam (figure 5). The results agree well with simulation (figure 4). The ground-breaking demonstration of ionization cooling presented here is a significant advance in the development of high-brightness muon beams. The seminal results presented in this paper encourage fur-

ther development of high-brightness muon beams as a tool for the investigation of the fundamental properties of matter.

Acknowledgements

The work described here was made possible by grants from the Science and Technology Facilities Council (UK), the Department of Energy and the National Science Foundation (USA), the Instituto Nazionale di Fisica Nucleare (Italy), the European Community under the European Commission Framework Programme 7 (AIDA project, grant agreement no. 262025, TIARA project, grant agreement no. 261905, and EuCARD), the Japan Society for the Promotion of Science, the National Research Foundation of Korea (No. NRF-2016R1A5A1013277), the Ministry of Education, Science and Technological Development of the Republic of Serbia, the Institute of High Energy Physics/Chinese Academy of Sciences fund for collaboration between the People's Republic of China and the USA and the Swiss National Science Foundation, in the framework of the SCOPES programme. We gratefully acknowledge all sources of support. We are grateful for the support given to us by the staff of the STFC Rutherford Appleton and Daresbury Laboratories. We acknowledge the use of Grid computing resources deployed and operated by GridPP in the UK, `http://www.gridpp.ac.uk/`.

Data Availability

The unprocessed and reconstructed data that support the findings of this study are publicly available on the GridPP computing Grid via the data DOIs:

- The MICE unprocessed data: `https://doi.org/doi:10.17633/rd.brunel.3179644`.
- The MICE reconstructed data: `https://doi.org/doi:10.17633/rd.brunel.5955850`.

Publications using the MICE data must contain the following statement: *We gratefully acknowledge the MICE collaboration for allowing us access to their data. Third-party results are not endorsed by the MICE collaboration.*

Software Availability

The MAUS software [63] that was used for reconstructing and analysing the MICE data is available at `https://doi.org/doi:10.17633/rd.brunel.8337542`.

Authorship

All authors contributed significantly to the design or construction of the apparatus or to the data-taking or analysis described here.

References

[1] E. O. Lawrence and M. S. Livingston, "The production of high speed protons without the use of high voltages," *Phys. Rev.* **38** (1931) 834.

[2] G. N. Lewis, M. S. Livingston, and E. O. Lawrence, "The Emission of Alpha-Particles from Various Targets Bombarded by Deutons of High Speed," *Phys. Rev.* **44** (1933) 55–56.

[3] E. O. Lawrence, "Method and apparatus for the acceleration of ions," *US Patent 1,948,384* (1934) .

[4] E. O. Lawrence and D. Cooksey, "On the apparatus for the multiple acceleration of light ions to high speed," *Phys. Rev.* **50** (1936) 1131–1140.

[5] R. Wideröe, "The 'gigator'–a proposed new circular accelerator for heavy particles," *Phys. Rev.* **72** (1947) 978.

[6] R. Wideröe, "Das Betatron," *Z. Angew. Phys.* **5** (1953) 187–200.

[7] D. V. Neuffer and R. B. Palmer, "A High-Energy High-Luminosity $\mu^+ - \mu^-$ Collider," in *Proceedings of the 4th European Particle Accelerator Conference*. 1994.

[8] S. Geer, "Neutrino beams from muon storage rings: Characteristics and physics potential," *Phys. Rev.* **D57** (1998) 6989–6997, arXiv:hep-ph/9712290.

[9] M. Apollonio *et al.*, "Oscillation physics with a neutrino factory," arXiv:hep-ph/0210192.

[10] M. M. Alsharo'a *et al.*, "Recent progress in neutrino factory and muon collider research within the muon collaboration," *Phys. Rev. ST Accel. Beams* **6** (2003) 081001.

[11] R. B. Palmer, "Muon Colliders," *Rev. Accel. Sci. Tech.* **7** (2014) 137–159.

[12] M. Boscolo, M. Antonelli, O. R. Blanco-Garcia, S. Guiducci, S. Liuzzo, P. Raimondi, and F. Collamati, "Low emittance muon accelerator studies with production from positrons on target," *Phys. Rev. Accel. Beams* **21** no. 6, (2018) 061005, arXiv:1803.06696 [physics.acc-ph].

[13] D. Neuffer and V. Shiltsev, "On the feasibility of a pulsed 14 TeV c.m.e. muon collider in the LHC tunnel," *JINST* **13** no. 10, (2018) T10003–T10003.

[14] T. Behnke, J. E. Brau, B. Foster, J. Fuster, M. Harrison, J. M. Paterson, M. Peskin, M. Stanitzki, N. Walker, and H. Yamamoto, "The International Linear Collider Technical Design Report - Volume 1: Executive Summary," arXiv:1306.6327 [physics.acc-ph].

[15] **CLIC and CLICdp** Collaboration, T. K. Charles *et al.*, "The Compact Linear Collider (CLIC) - 2018 Summary Report," *CERN Yellow Rep. Monogr.* **1802** (2018) 1–98, arXiv:1812.06018 [physics.acc-ph].

[16] **CLIC and CLICdp** Collaboration, P. Roloff, R. Franceschini, U. Schnoor, and A. Wulzer, "The Compact Linear e^+e^- Collider (CLIC): Physics Potential," arXiv:1812.07986 [hep-ex].

[17] **CLIC accelerator** Collaboration, M. Aicheler, P. N. Burrows, N. Catalan Lasheras, R. Corsini, M. Draper, J. Osborne, D. Schulte, S. Stapnes, and M. J. Stuart, "The Compact Linear Collider (CLIC) - Project Implementation Plan," arXiv:1903.08655 [physics.acc-ph].

[18] **FCC** Collaboration, A. Abada *et al.*, "FCC-ee: The Lepton Collider," *Eur. Phys. J. Special Topics* **228** (2019) 261–623.

[19] S. Myers, "The Large Hadron Collider 2008-2013," *Int. J. Mod. Phys.* **A28** (2013) 1330035.

[20] S. Y. Lee, *Accelerator Physics (Third Edition)*. World Scientific Publishing Co, 2012.

[21] S. Schröder *et al.*, "First laser cooling of relativistic ions in a storage ring," *Phys. Rev. Lett.* **64** (1990) 2901–2904.

[22] J. S. Hangst, M. Kristensen, J. S. Nielsen, O. Poulsen, J. P. Schiffer, and P. Shi, "Laser cooling of a stored ion beam to 1 mK," *Phys. Rev. Lett.* **67** (1991) 1238–1241.

[23] P. J. Channell, "Laser cooling of heavy ion beams," *Journal of Applied Physics* **52** no. 6, (1981) 3791–3793.

[24] D. Mohl, G. Petrucci, L. Thorndahl, and S. Van Der Meer, "Physics and Technique of Stochastic Cooling," *Phys. Rept.* **58** (1980) 73–119.

[25] J. Marriner, "Stochastic cooling overview," *Nucl. Instrum. Meth.* **A532** (2004) 11–18, arXiv:physics/0308044 [physics].

[26] V. V. Parkhomchuk and A. N. Skrinsky, "Electron cooling: 35 years of development," *Physics-Uspekhi* **43** no. 5, (2000) 433–452. http://stacks.iop.org/1063-7869/43/i=5/a=R01.

[27] M. Mühlbauer, H. Daniel, F. J. Hartmann, P. Hauser, F. Kottmann, C. Petitjean, W. Schott, D. Taqqu, and P. Wojciechowski, "Frictional cooling: Experimental results," *Hyperfine Interactions* **119** (1999) 305–310.

[28] H. Abramowicz, A. Caldwell, R. Galea, and S. Schlenstedt, "A Muon Collider scheme based on Frictional Cooling," *Nucl. Instrum. Meth.* **A546** (2005) 356–375, arXiv:physics/0410017.

[29] D. Taqqu, "Compression and Extraction of Stopped Muons," *Phys. Rev. Lett.* **97** no. 19, (2006) 194801.

[30] Y. Bao, A. Antognini, W. Bertl, M. Hildebrandt, K. S. Khaw, K. Kirch, A. Papa, C. Petitjean, F. M. Piegsa, S. Ritt, K. Sedlak, A. Stoykov, and D. Taqqu, "Muon cooling: Longitudinal compression," *Phys. Rev. Lett.* **112** (2014) 224801.

[31] A. N. Skrinsky and V. V. Parkhomchuk, "Cooling Methods for Beams of Charged Particles. (In Russian)," *Sov. J. Part. Nucl.* **12** (1981) 223–247.

[32] D. Neuffer, "Principles and Applications of Muon Cooling," *Part. Accel.* **14** (1983) 75–90.

[33] C. T. Rogers, D. Stratakis, G. Prior, S. Gilardoni, D. Neuffer, P. Snopok, A. Alekou, and J. Pasternak, "Muon front end for the neutrino factory," *Phys. Rev. ST Accel. Beams* **16** (2013) 040104.

[34] D. Stratakis and R. B. Palmer, "Rectilinear six-dimensional ionization cooling channel for a muon collider: A theoretical and numerical study," *Phys. Rev. ST Accel. Beams* **18** no. 3, (2015) 031003.

[35] D. Neuffer, H. Sayed, J. Acosta, D. Summers, and T. Hart, "Final Cooling for a High-Energy High-Luminosity Lepton Collider," *JINST* **12** no. 07, (2017) T07003, arXiv:1612.08960 [physics.acc-ph].

[36] S. Bae *et al.*, "First muon acceleration using a radio frequency accelerator," *Phys. Rev. Accel. Beams* **21** no. 5, (2018) 050101, arXiv:1803.07891 [physics.acc-ph].

[37] Y. Mori, Y. Ishi, Y. Kuriyama, Y. Sakurai, T. Uesugi, K. Okabe, and I. Sakai, "Neutron Source with Emittance Recovery Internal Target," in *Proceedings of the 23rd Particle Accelerator Conference*. 2009. http://accelconf.web.cern.ch/AccelConf/PAC2009/papers/th4gac04.pdf.

[38] **MICE** Collaboration, "International Muon Ionization Cooling Experiment." http://mice.iit.edu.

[39] G. Penn and J. S. Wurtele, "Beam envelope equations for cooling of muons in solenoid fields," *Phys. Rev. Lett.* **85** (2000) 764.

[40] E. B. Holzer, "Figure of merit for muon cooling – an algorithm for particle counting in coupled phase planes," *Nucl. Instrum. Meth.* **A532** (2004) 270–274.

[41] C. Rogers, *Beam Dynamics in an Ionisation Cooling Channel*. PhD dissertation, Imperial College, London, 2008.

[42] Y. Mack and M. Rosenblatt, "Multivariate k-nearest neighbor density estimates," *Journal of Multivariate Analysis* **9** no. 1, (1979) 1 – 15.

[43] F. Drielsma, *Measurement of the increase in phase space density of a muon beam through ionization cooling*. PhD thesis, University of Geneva, 2018.

[44] **MICE** Collaboration, M. Bogomilov *et al.*, "The MICE Muon Beam on ISIS and the beam-line instrumentation of the Muon Ionization Cooling Experiment," *JINST* **7** (2012) P05009, arXiv:1203.4089 [physics.acc-ph].

[45] **MICE** Collaboration, D. Adams *et al.*, "Characterisation of the muon beams for the Muon Ionisation Cooling Experiment," *Eur. Phys. J.* **C73** no. 10, (2013) 2582, arXiv:1306.1509 [physics.acc-ph].

[46] **MICE** Collaboration, M. Bogomilov *et al.*, "Pion Contamination in the MICE Muon Beam," *JINST* **11** no. 03, (2016) P03001, arXiv:1511.00556 [physics.ins-det].

[47] C. Booth, P. Hodgson, J. Langlands, E. Overton, M. Robinson, P. Smith, G. Barber, K. Long, B. Shepherd, E. Capocci, C. MacWaters, and J. Tarrant, "The design and performance of an improved target for MICE," *JINST* **11** no. 05, (2016) P05006–P05006.

[48] J. Thomason, "The ISIS Spallation Neutron and Muon Source - The first thirty-three years," *Nucl. Instrum. Meth.* **A917** (2019) 61 – 67.

[49] **MICE** Collaboration, V. Bayliss *et al.*, "The liquid-hydrogen absorber for MICE," *JINST* **13** no. 09, (2018) T09008, arXiv:1807.03019 [physics.acc-ph].

[50] D. Stratakis, R. B. Palmer, and D. P. Grote, "Influence of space-charge fields on the cooling process of muon beams," *Phys. Rev. ST Accel. Beams* **18** (2015) 044201.

[51] **MICE** Collaboration, V. Blackmore *et al.*, "First particle-by-particle measurement of emittance in the muon ionization cooling experiment," *Eur. Phys. J. C* **79** no. 3, (2019) 257.

[52] **MICE** Collaboration, R. Bertoni *et al.*, "The design and commissioning of the MICE upstream time-of-flight system," *Nucl. Instrum. Meth.* **A615** (2010) 14–26, arXiv:1001.4426 [physics.ins-det].

[53] R. Bertoni, M. Bonesini, A. deBari, G. Cecchet, Y. Karadzhov, and R. Mazza, "The construction of the MICE TOF2 detector," *MICE Technical Note 254* (2010) . http://mice.iit.edu/micenotes/public/pdf/MICE0286/MICE0286.pdf.

[54] L. Cremaldi, D. Sanders, P. Sonnek, D. Summers, and J. Reidy, "A cherenkov radiation detector with high density aerogels," *IEEE Transactions on Nuclear Science* **56** (2009) 1475 – 1478.

[55] M. Ellis *et al.*, "The Design, construction and performance of the MICE scintillating fibre trackers," *Nucl. Instrum. Meth.* **A659** (2011) 136–153, arXiv:1005.3491 [physics.ins-det].

[56] A. Dobbs, C. Hunt, K. Long, E. Santos, M. A. Uchida, P. Kyberd, C. Heidt, S. Blot, and E. Overton, "The reconstruction software for the MICE scintillating fibre trackers," *JINST* **11** no. 12, (2016) T12001, arXiv:1610.05161 [physics.ins-det].

[57] **MICE** Collaboration, D. Adams *et al.*, "Electron-Muon Ranger: performance in the MICE Muon Beam," *JINST* **10** no. 12, (2015) P12012, arXiv:1510.08306 [physics.ins-det].

[58] R. Asfandiyarov *et al.*, "The design and construction of the MICE Electron-Muon Ranger," *JINST* **11** no. 10, (2016) T10007, arXiv:1607.04955 [physics.ins-det].

[59] M. Petroff and M. Stapelbroek, "Photon-Counting Solid-State Photomultiplier," *IEEE Transactions on Nuclear Science* **36** no. 1, Part 1, (1989) 158–162.

[60] M. Petroff and M. Atac, "High-Energy Particle Tracking using Scintillation Fibers and Solid-State Photomultipliers," *IEEE Transactions on Nuclear Science* **36** no. 1, Part 1, (1989) 163–164.

[61] S. Agostinelli *et al.*, "GEANT4: A Simulation toolkit," *Nucl. Instrum. Meth.* **A506** (2003) 250–303.

[62] J. Allison *et al.*, "Geant4 developments and applications," *IEEE Transactions on Nuclear Science* **53** (2006) 270.

[63] R. Asfandiyarov *et al.*, "MAUS: The MICE Analysis User Software," *JINST* **14** (2019) T04005–T04005, arXiv:1812.02674 [physics.comp-ph].

Methods

Data-taking and reconstruction

Data were buffered in the front-end electronics and read out after each target actuation. Data storage was triggered by a coincidence of signals in the photmultiplier tubes (PMTs) serving a single scintillator slab in TOF1. The data recorded in response to a particular trigger are referred to as a 'particle event'.

Each TOF station was composed of a number of scintillator slabs that were read out using a pair of PMTs, one mounted at each end of the slab. The reconstruction of the data began with the search for coincidences in the signals from the two PMTs serving each slab in each TOF plane. Such coincidences were referred to as 'slab hits'. 'Space points' were then formed from the intersection of slab hits in the x and y projections of each TOF station separately. The position and time at which a particle giving rise to the space point crossed the TOF station was then calculated using the slab position and the times measured in each of the PMTs. The relative timing of TOF0 and TOF1 was calibrated relative to the observed time taken for electrons to pass between the two detectors, on the assumption that they travelled at the speed of light.

Signals in the tracker readout were collected to reconstruct the helical trajectories ('tracks') of charged particles in the upstream and downstream trackers (TKU and TKD respectively). Multiple Coulomb scattering introduced significant uncertainties in the reconstruction of the helical trajectory of tracks with a bending radius less than 5 mm. For this class of track momentum was deduced by combining the tracker measurement with the measurements from nearby detectors. Track-fit quality was characterised by the χ^2 per degree-of-freedom

$$\chi^2_{\rm df} = \frac{1}{n}\sum_i \frac{\delta x_i^2}{\sigma_i^2} \tag{8}$$

where δx_i is the distance between the fitted track and the measured signal in the i^{th} tracker plane, σ_i is the resolution of the position measurement in the tracker planes and n is the number of planes that had a signal used in the track reconstruction. Further details of the reconstruction and simulation may be found in [63].

Beam selection

Measurements made in the instrumentation upstream of the absorber were used to select the input beam for the study of ionization cooling presented in this paper. The input beam (the 'upstream sample') was composed of those events that satisfied the following criteria:

- Exactly one space point was found in TOF0 and TOF1 and exactly one track in TKU;
- The track in TKU had $\chi^2_{\rm df} < 8$ and was contained within the 150 mm fiducial radius over the full length of the tracker;
- The track in TKU had a reconstructed momentum in the range 135–145 MeV/c corresponding to the momentum acceptance of the cooling cell;
- The time-of-flight between TOF0 and TOF1 was consistent with that of a muon given the momentum measured in TKU; and
- The radius at which the track in TKU passed through the diffuser was smaller than the diffuser aperture.

The beam emerging from the cooling cell (the 'downstream sample') was characterised using the subset of the upstream sample that satisfied the following criteria:

- Exactly one track was found in TKD; and
- The track in TKD had a $\chi^2_{\rm df} < 8$ and was contained within the 150 mm fiducial radius of TKD over the full length of the tracker.

The same sample-selection criteria were used to select events from the simulation of the experiment, which includes a reconstruction of the electronics signals expected for the simulated particles.

Correction for detector effects

The amplitude distributions obtained from the upstream and downstream samples were corrected for the effects of detector efficiency and resolution and to take account of migration of events between amplitude bins. The corrected number of events in a bin, N_i^{corr}, was calculated from the raw number of events, N_j^{raw}, using

$$N_i^{corr} = E_i \sum_j S_{ij} N_j^{raw}, \tag{9}$$

where E_i is the efficiency-correction factor and S_{ij} accounts for detector resolution and event migration. E_i and S_{ij} were estimated from the simulation of the experiment. The uncorrected and corrected amplitude distributions for a particular configuration are shown in figure 1. The correction is small relative to the ionization cooling effect; the ionization cooling effect is clear even in the uncorrected distributions.

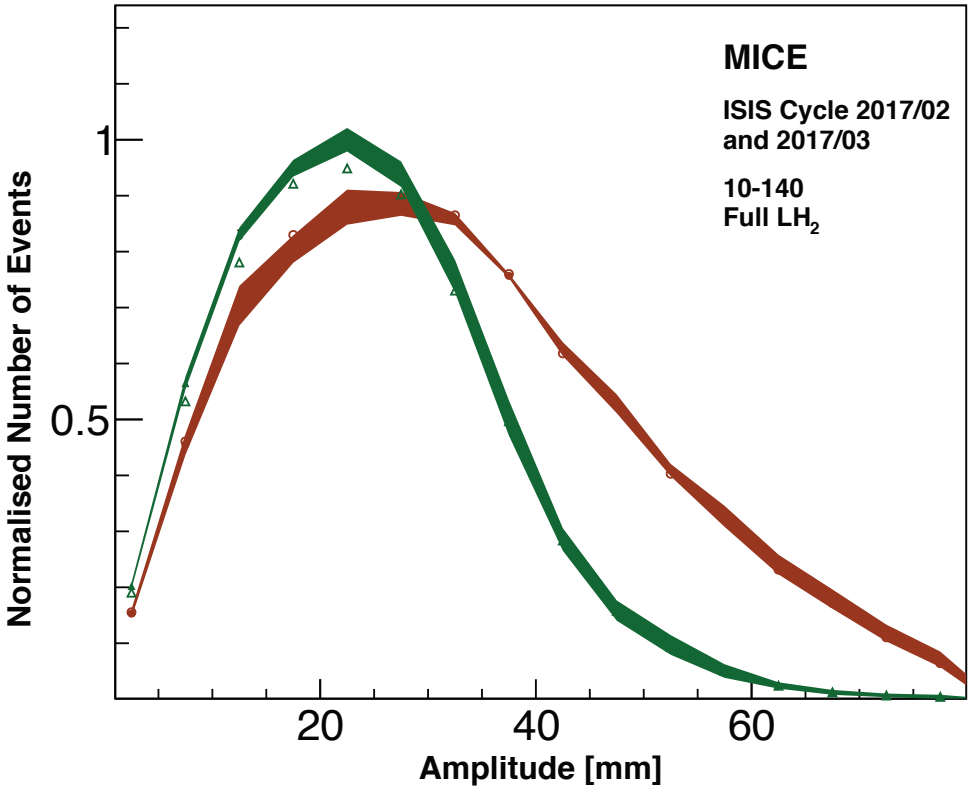

Figure 1: Distribution of amplitudes with corrected and uncorrected distribution shown for the 10-140 LH_2 full configuration. The uncorrected data is shown by open points while the corrected data is shown by filled points. The upstream distribution is shown by orange circles while the downstream distribution is shown by green triangles. Systematic uncertainty is shown by coloured bands. Statistical error is shown by bars and is just visible for a few points.

The MICE collaboration

M. Bogomilov, R. Tsenov, G. Vankova-Kirilova
Department of Atomic Physics, St. Kliment Ohridski University of Sofia, Sofia, Bulgaria

Y. P. Song, J. Y. Tang
Institute of High Energy Physics, Chinese Academy of Sciences, Beijing, China

Z. H. Li
Sichuan University, China

R. Bertoni, M. Bonesini, F. Chignoli, R. Mazza
Sezione INFN Milano Bicocca, Dipartimento di Fisica G. Occhialini, Milano, Italy

V. Palladino
Sezione INFN Napoli and Dipartimento di Fisica, Università Federico II, Complesso Universitario di Monte S. Angelo, Napoli, Italy

A. de Bari
Sezione INFN Pavia and Dipartimento di Fisica, Pavia, Italy

D. Orestano, L. Tortora
INFN Sezione di Roma Tre and Dipartimento di Matematica e Fisica, Università Roma Tre, Italy

Y. Kuno, H. Sakamoto[1], A. Sato
Osaka University, Graduate School of Science, Department of Physics, Toyonaka, Osaka, Japan

S. Ishimoto
High Energy Accelerator Research Organization (KEK), Institute of Particle and Nuclear Studies, Tsukuba, Ibaraki, Japan

M. Chung, C. K. Sung
UNIST, Ulsan, Korea

F. Filthaut[2]
Nikhef, Amsterdam, The Netherlands

D. Jokovic, D. Maletic, M. Savic
Institute of Physics, University of Belgrade, Serbia

N. Jovancevic, J. Nikolov
Faculty of Sciences, University of Novi Sad, Serbia

[1] Current address RIKEN 2-1 Horosawa, Wako, Saitama 351-0198, Japan
[2] Also at Radboud University, Nijmegen, The Netherlands

M. Vretenar, S. Ramberger
CERN, Esplanade des Particules 1, P.O. Box 1211, Geneva 23, Switzerland

R. Asfandiyarov, A. Blondel, F. Drielsma, Y. Karadzhov
DPNC, Section de Physique, Université de Genève, Geneva, Switzerland

G. Charnley, N. Collomb, K. Dumbell, A. Gallagher, A. Grant, S. Griffiths, T. Hartnett, B. Martlew, A. Moss, A. Muir, I. Mullacrane, A. Oates, P. Owens, G. Stokes, P. Warburton, C. White
STFC Daresbury Laboratory, Daresbury, Cheshire, UK

D. Adams, V. Bayliss, J. Boehm, T. W. Bradshaw, C. Brown[3], M. Courthold, J. Govans, M. Hills, J.-B. Lagrange, C. Macwaters, A. Nichols, R. Preece, S. Ricciardi, C. Rogers, T. Stanley, J. Tarrant, M. Tucker, S. Watson[4], A. Wilson
STFC Rutherford Appleton Laboratory, Harwell Oxford, Didcot, UK

R. Bayes[5], J. C. Nugent, F. J. P. Soler
School of Physics and Astronomy, Kelvin Building, The University of Glasgow, Glasgow, UK

R. Gamet, P. Cooke
Department of Physics, University of Liverpool, Liverpool, UK

V. J. Blackmore, D. Colling, A. Dobbs[6], P. Dornan, P. Franchini, C. Hunt[7], P. B. Jurj, A. Kurup, K. Long, J. Martyniak, S. Middleton[8], J. Pasternak, M. A. Uchida[9]
Department of Physics, Blackett Laboratory, Imperial College London, London, UK

J. H. Cobb
Department of Physics, University of Oxford, Denys Wilkinson Building, Oxford, UK

C. N. Booth, P. Hodgson, J. Langlands, E. Overton[10], V. Pec, P. J. Smith, S. Wilbur
Department of Physics and Astronomy, University of Sheffield, Sheffield, UK

G. T. Chatzitheodoridis[11,12], A. J. Dick[12], K. Ronald[12], C. G. Whyte[12], A. R. Young[12]
SUPA and the Department of Physics, University of Strathclyde, Glasgow, UK

S. Boyd, J. R. Greis, T. Lord, C. Pidcott[13], I. Taylor[14]
Department of Physics, University of Warwick, Coventry, UK

[3]Also at Brunel University, Uxbridge, UB8 3PH, UK
[4]Current address ATC, Royal Observatory Edinburgh, Blackford Hill, Edinburgh EH9 3HJ
[5]Current address Laurentian University, 935 Ramsey Lake Road, Sudbury, ON, Canada
[6]Current address OPERA Simulation Software, Network House, Langford Locks, Kidlington, Oxfordshire, OX5 1LH, UK
[7]Current address CERN, Esplanade des Particules 1, P.O. Box, 1211 Geneva 23, Switzerland.
[8]Current address School of Physics and Astronomy, University of Manchester, Oxford Road, Manchester M13 9PL, UK
[9]Current address Rutherford Building, Cavendish Laboratory, JJ Thomson Avenue, Cambridge CB3 0HE, UK
[10]Current address Arm, City Gate, 8 St Mary's Gate, Sheffield, S1 4LW, United Kingdom
[11]Also at School of Physics and Astronomy, Kelvin Building, The University of Glasgow, Glasgow, UK
[12]Also at Cockcroft Institute, Daresbury Laboratory, Sci-Tech Daresbury, Daresbury, Warrington, WA4 4AD, UK
[13]Current address Department of Physics and Astronomy, University of Sheffield, Sheffield, UK
[14]Current address Defence Science and Technology Laboratory, Salisbury, SP4 0JQ, UK

M. Ellis[15], R.B.S. Gardener, P. Kyberd, J. J. Nebrensky
Brunel University, Uxbridge, UB8 3PH, UK

M. Palmer, H. Witte
Brookhaven National Laboratory, NY, USA

D. Adey[16], A. D. Bross, D. Bowring, P. Hanlet, A. Liu[17], D. Neuffer, M. Popovic, P. Rubinov
Fermilab, PO Box 500, Batavia IL 60510-5011, USA

A. DeMello, S. Gourlay, A. Lambert, D. Li, T. Luo, S. Prestemon, S. Virostek
Lawrence Berkeley National Laboratory, Berkeley, CA, USA

B. Freemire[17], D. M. Kaplan, T. A. Mohayai[18], D. Rajaram[19], P. Snopok, Y. Torun
Illinois Institute of Technology, Chicago, IL, USA

L. M. Cremaldi, D. A. Sanders, D. J. Summers
University of Mississippi, Oxford, MS, USA

L. R. Coney[20], G. G. Hanson, C. Heidt.
University of California, Riverside, CA, USA

[15]Current address Westpac Group, Sydney, Australia
[16]Current address Institute of High Energy Physics, Chinese Academy of Sciences, Bejing, China
[17]Current address Euclid Techlabs, Bolingbrook, Illinois 60440, USA
[18]Current address Fermilab, PO Box 500, Batavia IL 60510-5011, USA
[19]Current address Illinois Institute of Technology, College of Science, Robert A. Pritzker Science Center, 3105 South Dearborn, Chicago, IL 60616P, USA
[20]Current address European Spallation Source ERIC, Box 176, SE-221 00 Lund, Sweden